

# Operational mode transition in a rotating detonation engine\*

Zhi-di LEI<sup>1</sup>, Zheng-wu CHEN<sup>2</sup>, Xiao-quan YANG<sup>†‡1</sup>, Jue DING<sup>†‡1</sup>, Pei-fen WENG<sup>1</sup>

<sup>1</sup>Shanghai Key Laboratory of Mechanics in Energy Engineering, Shanghai Institute of Applied Mathematics and Mechanics, School of Mechanics and Engineering Science, Shanghai University, Shanghai 200072, China

<sup>2</sup>Key Laboratory of Aerodynamic Noise Control, China Aerodynamics Research and Development Center, Mianyang 621000, China

<sup>†</sup>E-mail: quanshui@shu.edu.cn; dingjue\_lu@shu.edu.cn

Received July 23, 2019; Revision accepted Jan. 21, 2020; Crosschecked July 15, 2020

**Abstract:** The relationship between the number of detonation waves and the evolution process of the flow field in a rotating detonation engine was investigated through a numerical analysis. The simulations were based on the Euler equation and a detailed chemical reaction model. In the given engine model, the flow-field evolution became unstable when a single detonation wave was released. New detonation waves formed spontaneously, changing the operational mode from single-wave to four-wave. However, when two or three detonation waves were released, the flow field evolved in a quasi-steady manner. Further study revealed that the newly formed detonation wave resulted from an accelerated chemical reaction on the contact surface between the detonation products and the reactive mixture. To satisfy the stable propagation requirements of detonation waves, we proposed a parameter called  $N_L$ , which can be compared with the number of detonation waves in the combustor to predict the evolution (quasi-stable or unstable) of the flow field. Finally, we verified the effectiveness of  $N_L$  in a redesigned engine. This study may assist the operational mode control in rotating detonation engine experiments.

**Key words:** Rotating detonation engine; Chemical reaction; Multiple detonation waves; Stability

<https://doi.org/10.1631/jzus.A1900349>

**CLC number:** V231

## 1 Introduction

Unlike ordinary isobaric combustion in traditional aerospace engines, detonation is a chemical reaction induced by a shock wave. Owing to its fast chemical reaction rate, detonation approximates a constant-volume process in which the entropy of det-

onation is less than that of isobaric combustion. For this reason, detonation has a high thermodynamic efficiency. In recent years, various engines using detonation for energy release have been explored for their application prospects, including the pulse detonation engine, the oblique detonation wave engine, and the rotating detonation engine (RDE). RDE is considered as one of the most promising aerospace power devices, because it is simply structured and a single ignition provides a sustained thrust in its compact combustor. In addition, it is possible to build combined-cycle RDE (Wolański, 2011; Zhang TT et al., 2019).

The practical application of RDEs has attracted significant research interest since the 1960s, shortly after Voitsekhoivskii (1959) achieved

<sup>‡</sup> Corresponding author

\* Project supported by the National Natural Science Foundation of China (No. 11702329), the Open Project Program of the Key Laboratory of Aerodynamic Noise Control of China Aerodynamics Research and Development Center (CARD) (No. ANCL20180103), the CARD Fundamental and Frontier Technology Research Fund (No. PJD20180143), and the Open Project Program of Rotor Aerodynamics Key Laboratory (No. RAL20180403), China

 ORCID: Zhi-di LEI, <https://orcid.org/0000-0003-2520-8302>

© Zhejiang University and Springer-Verlag GmbH Germany, part of Springer Nature 2020

short-lived rotating detonation. Many aspects of RDEs have been reported, including the engine ignition characteristics (Peng et al., 2015; Li et al., 2018), flow-field structure (Oran et al., 1998; Naples et al., 2013), stability of detonation waves (DWs) in the combustor (Wu et al., 2014; Anand et al., 2015), operational modes in RDEs (Bykovskii and Vedernikov, 1996; Frolov et al., 2015; Wang et al., 2015), and the effect of imperfect mixing (Nordeen et al., 2016). Most previous studies on RDEs assumed a single DW in the annular detonation combustor. Recent studies have shown that in some cases, the engine can maintain multiple DWs (Bykovskii et al., 2006; Frolov et al., 2015; Lin et al., 2015; Yao and Wang, 2016; George et al., 2017). When implemented as a power device, an RDE must operate stably in the desired operational mode (defined by the number and propagating direction of DWs in the combustor). However, the operational mode is not always fixed. The number of DWs may instantaneously change when the operational or injection conditions vary for any reason (Bykovskii et al., 2006; Falempin and Naour, 2009; Frolov et al., 2015; George et al., 2017; Deng et al., 2018). Bykovskii et al. (2006) analyzed how continuous spin detonation is affected by physical, chemical, and geometric parameters, and reported a control method for continuous spin detonation. Falempin and Naour (2009) found that the number of DWs in the combustion chamber is influenced by factors such as the mass flow rate, size of the combustion chamber, and fuel properties. Frolov et al. (2015) experimentally showed that by setting appropriate obstacles in the outlet of the combustion chamber, the number of DWs can be increased to enhance the thrust of the engine. George et al. (2017) proved that the existence and multiplicity of rotating DWs can be feasibly predicted from the combustor geometry and the mixture-cell width. Deng et al. (2018) demonstrated the feasibility of transforming the operational modes by changing the chemical equivalence ratio of the fuel in a given engine. Anand et al. (2015) reported that the number of DWs can spontaneously and unpredictably change in a combustor with a given geometry, causing large instabilities. Understanding the mechanism of such operational mode changes is essential, yet only Yao and Wang (2016) have thus far studied the spontaneous formation process of new DW fronts. They attributed the spontaneously formed DWs to collisions between

compressive waves (Yao et al., 2015). However, Deng et al. (2018) identified other possible causes of the newly generated DWs.

The above discussion implies that operational mode changes are related to the number of DWs. Therefore, predicting and preventing this mode change are essential for engineering applications of RDEs. To this end, we investigated the multiplicity phenomenon in the rotating detonation flow field of an engine with different numbers of initial DWs, from ignition to stable operation. The reaction rate of the pre-mixed hydrogen, oxygen, and nitrogen mixture was calculated using a detailed chemical reaction model. Next, we analyzed the evolution processes of the rotating detonation flow field. At the end of this study, we quantitatively related the number of DWs to the evolution mode in the combustor of an RDE.

## 2 Physical model and numerical method

### 2.1 Physical model and computational domain

Fig. 1 is a schematic of the modeled RDE combustor and its computational domain. The annular RDE combustor is 100 mm long, and its inner and outer diameters are 90.5 and 100.5 mm, respectively. The mixture is injected into the combustor from the bottom inlet. DW continuously consumes the fresh injected mixture in the circumferential direction near the inlet section, and the combustion products are ejected along the axial direction from the top outlet. The chamber's radial height is assumed negligible relative to its mean radius. Ignoring the radial effect, we can reduce the 3D field to a 2D domain. The combustion chamber is assumed to have no thickness, and is modeled as a line segment  $OB$  rotating around the central axis. The computational domain

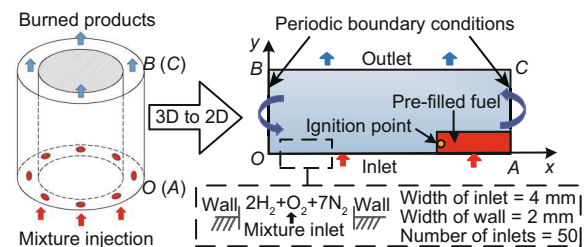


Fig. 1 Schematic of the combustion chamber, computational domain, and injector

$OACB$  is obtained by cutting along the line  $OB$  and unwrapping the annulus in the azimuthal direction, as depicted in Fig. 1. Before the model is deformed,  $OB$  and  $AC$  are identical lines connected by setting periodic boundary conditions. This simplification is widely used by Deng et al. (2018) and Fujii et al. (2017).  $OA$  is the mixture injection inlet located at the bottom, and  $BC$  is the open exit.  $OB$  and  $BC$  are 100 and 300 mm long, respectively.

## 2.2 Governing equations and computational methods

The governing equations are the unsteady Euler equations coupled with detailed chemical reactions.

$$\frac{\partial \mathbf{u}}{\partial t} + \frac{\partial \mathbf{F}}{\partial x_i} = \mathbf{Q}, \quad (1)$$

$$\mathbf{u} = [\rho, \rho \mathbf{U}, \rho E, \rho Y_i]^T, \quad (2)$$

$$\mathbf{F} = [\rho \mathbf{U}, \rho \mathbf{U} \mathbf{U} + p, \rho E \mathbf{U} + \mathbf{U} p, \rho Y_i \mathbf{U}]^T, \quad (3)$$

$$\mathbf{Q} = [0, \mathbf{0}, \dot{\omega}_T, \dot{\omega}_i]^T, \quad (4)$$

where  $t$  is the time,  $x_i$  ( $i=1, 2, 3$ ) denote the  $x$ -,  $y$ -, and  $z$ -axes in the Cartesian plane, respectively,  $\mathbf{U}$  is the velocity vector,  $\rho$  is the fluid density, and  $p$  is the pressure.  $Y_i$  is the mass fraction of species  $i$  and  $\sum Y_i = 1$ .  $E$  is the non-chemical total energy, given by

$$E = h_s - p/\rho + \frac{1}{2} \|\mathbf{U}\|^2. \quad (5)$$

The sensible enthalpy  $h_s$  is related to the temperature  $T$  as

$$h_s = \int_{T_0}^T c_p dT, \quad (6)$$

where  $c_p$  is the specific heat capacity at constant pressure and  $T_0$  is the initial temperature. In the energy equation,  $\dot{\omega}_T$  is computed as

$$\dot{\omega}_T = \sum_{i=1}^N \dot{\omega}_i h_{f,i}^o, \quad (7)$$

where  $\dot{\omega}_i$  and  $h_{f,i}^o$  are the production/consumption rate and formation enthalpy of species  $i$ , respectively. To compute the source terms in species and energy equations, we require appropriate chemical kinetics models. Here, the hydrogen, oxygen, and nitrogen chemical reactions are described using a detailed chemistry reaction model (Hippler et al., 1995;

Marinov, 1995), which contains 27 reversible reactions of 10 chemical species. The chemical source term  $\dot{\omega}_i$  can be written in general form as

$$\dot{\omega}_i = W_i \sum_{n=1}^N (\gamma''_{ni} - \gamma'_{ni}) (k_{fn} \prod_{i=1}^I X_i^{\gamma'_{ni}} - k_{bn} \prod_{i=1}^I X_i^{\gamma''_{ni}}), \quad (8)$$

where  $\gamma'_{ni}$  and  $\gamma''_{ni}$  denote the stoichiometric coefficients of the reactants and products, respectively.  $I$  is the total number of reactions.  $W_i$  is the molecular weight of species  $i$  and  $N$  is the total number of elementary reactions.  $k_{fn}$  and  $k_{bn}$  are the forward and backward specific reaction rate constants, respectively.  $X_i$  is the molar concentration of  $i$ . The forward reaction rate constants are defined by the Arrhenius law:

$$k_{fn} = A_{fn} T^{\beta_{fn}} \exp\left(-\frac{E_{fn}}{RT}\right), \quad (9)$$

where  $A_{fn}$  is the pre-exponential factor,  $\beta_{fn}$  is the temperature exponent,  $E_{fn}$  is the activation energy, and  $R$  is the universal gas constant.

The governing equations are solved using the time-splitting approach (also known as the fractional step method), which decouples the transport and reactive processes. The chemical reaction model is treated as a system of stiff ordinary differential equations solved using the semi-implicit Bulirsch-Stoer method (SIBS) (Bader and Deuffhard, 1983). After computing the source terms for the species and energy equations, the computation of the dynamic fluid system is initiated. To accurately capture the shock waves and discontinuities, the convective terms are evaluated using the second-order central-upwind scheme of Kurganov et al. (2001). The time evolution of the flow field is calculated using the second-order Crank-Nicolson scheme. The Courant-Friedrichs-Levy number is assumed constant at 0.1.

## 2.3 Boundary conditions

The injection condition significantly influences the rotating detonation flow field and stability of an RDE. In this study, the mixture injection is simulated using the interval injection method, which simulates the actual injection conditions better than the traditional whole-area injection method. In particular, as the interval injection treats each inlet grid as a small injection orifice, it can reflect the flow-field characteristics (Yao et al., 2015, 2017; Fujii et al.,

2017; Deng et al., 2018). The applied settings are shown in Fig. 1. Each injection area is 4 mm wide. The width of each wall separating the injection area is 2 mm. The injection area is connected to a gas tank held under constant total pressure  $p_{st} = 10$  atm (1 atm=101 325 Pa) and total temperature  $T_{st} = 600$  K, which provide the premixed hydrogen, oxygen, and nitrogen mixtures for the combustor at a molar ratio of 2 : 1 : 7. Treating the injection process as a 1D isentropic flow, the inlet boundary conditions ( $p_{in}$ ,  $T_{in}$ , and  $u_{in}$ ) are assumed to depend on pressure  $p$  in the combustor near the lower inlet. If  $p > p_{st}$ , the reactive mixture cannot be injected into the combustion chamber. The inlet boundary is then treated as a solid wall boundary:

$$p_{in} = p, \quad T_{in} = T, \quad u_{in} = 0, \quad (10)$$

where  $u_{in}$  is the normal value of the velocity field at the boundary. If  $p_{cr} \leq p \leq p_{st}$ , where  $p_{cr} = p_{st} \left( \frac{2}{\gamma+1} \right)^{\frac{\gamma}{\gamma-1}}$ , the flow is given by the isentropic solutions:

$$p_{in} = p, \quad (11)$$

$$T_{in} = T_{st} \left( \frac{p_{in}}{p_{st}} \right)^{\frac{\gamma-1}{\gamma}}, \quad (12)$$

$$u_{in} = \sqrt{\frac{2\gamma}{\gamma-1} RT_{st} \left[ 1 - \left( \frac{p_{in}}{p_{st}} \right)^{\frac{\gamma-1}{\gamma}} \right]}, \quad (13)$$

where  $\gamma$  is the specific heat ratio of the mixture. If  $p \leq p_{cr}$ , the flow is choked, so  $p_{in} = p_{cr}$ . Eqs. (12) and (13) provide the temperature and velocity at the boundary, respectively. Similar entry conditions were set by Schwer and Kailasanath (2011) and Fujii et al. (2017). The initial conditions in the computational domain are  $p = 1$  atm and  $T = 293$  K. An adiabatic wall condition is set in the lower end area, which has no nozzle. The *OB* and *AC* edges are assumed as periodic boundaries. At the outlet *BC*, the flow is supersonic and all physical variables are extrapolated from the internal field. The pressure  $p_{out}$  at the outlet boundary *BC* is relaxed to the extrapolation limit  $p_{\infty}$ :

$$p_{out} = p(1-r) + p_{\infty}r, \quad (14)$$

where  $p$  is the pressure near the outlet,  $p_{\infty}$  is the ambient pressure (1 atm), and  $r$  is the relaxation rate coefficient (0.05). This outlet boundary condition was suggested by Gamezo et al. (1999), and

proven suitable for RDE simulations in a previous numerical study (Yao and Wang, 2016). In the experiments, RDE is often initiated by a pre-detonator, which tangentially “injects” the DW into the combustor. To emulate the function of a pre-detonator, we set a small area at a high temperature and high pressure, which rapidly detonates the pre-filling fuel to create the initial DWs. This inlet area is illustrated in Fig. 1. When more initial DWs are needed, more ignition points and alternating reactant-inert strips are set. In the calculation results, this method creates DWs in the combustion chamber within 20  $\mu$ s, as occurs in actual pre-detonators. Moreover, the number of initial DWs can be controlled by changing the number of ignition positions.

## 3 Results

### 3.1 Code validation and grid independence analysis

In this section, the developed code is validated in two cases, the shock tube case and the detonation case. The shock tube case examines the so-called Sod test problem (Sod, 1978), while the detonation case validates the chemical models and grid independence.

In the shock tube case, the numerical scheme and its coding are verified via shock wave propagation in a channel. The wave is generated by expanding the compressed left region and propagating it to the right region. The initial conditions ( $\gamma = 1.4$ ,  $p_L = 1$ ,  $\rho_L = 1$ ,  $p_R = 0.1$ ,  $\rho_R = 0.125$ ) are proposed by Sod (1978), where  $p_L$  and  $\rho_L$  denote the pressure and density of the left region of the shock tube, respectively, and  $p_R$  and  $\rho_R$  denote the pressure and density of the right region of the shock tube, respectively. The 1D calculation results and the analytical solution are compared in Fig. 2. As confirmed in the figure, the numerical solution agrees with the analytical solution, and develops no oscillations.

The detonation study verifies the grid independence and chemical models in a 2D detonation tube. In this study, the orthogonal grid size is varied as 0.2, 0.5, and 1.0 mm. The rectangular calculation domain is filled with a stoichiometric hydrogen-air mixture at the initial pressure ( $p = 1$  atm) and  $T = 293$  K. The DWs are triggered by hotspots. Table 1 compares the simulation results, theoretical

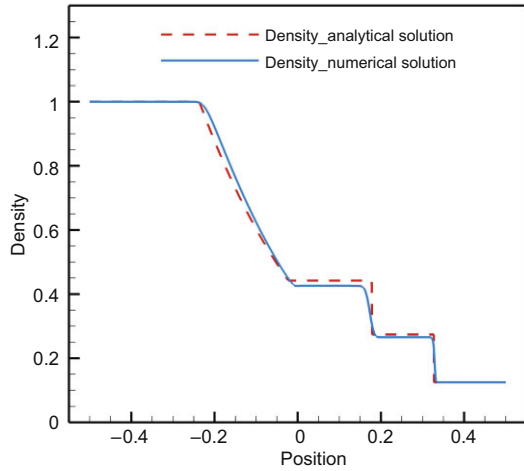


**Fig. 2** Comparison of numerically calculated density and the analytical solution of the Sod test problem at time  $t = 0.2$  units

**Table 1** Theoretical, experimental, and simulated detonation wave velocities

Item	Grid size (mm)	$u_{\text{DW}}$ (m/s)	Error
Simulation	1.0	1960.0	0.835%
	0.5	1970.6	0.299%
	0.2	1971.9	0.233%
Theoretical solution	—	1976.5	—
Experimental data	—	1970.0	—

$u_{\text{DW}}$ : velocity of detonation wave; error: proportional difference between the simulated and theoretical  $u_{\text{DW}}$  values

values (Deng et al., 2018), and experimental results (Ginsberg et al., 1994). The DW velocity approximates the theoretical and experimental values, confirming the grid independence of the detonation velocity and the correctness of the chemical models. Furthermore, a one-wave stable rotating detonation field with chemical reactions and fuel injection is simulated in a 2D RDE case. The pressure contours computed on the 0.2-mm and 0.5-mm grids are compared in Fig. 3. Although the 0.2-mm grid system provides a more detailed structure of the flow field than the coarser grid, it does not remarkably improve the essential features of the rotating detonation field, such as the pressure distribution field. Both the DW heights and operation frequencies are also similar on the two grids, consolidating the numerical convergence and grid independency of the simulations. Because this study aims to investigate the evolution process of the whole flow field, rather than the details of the wave structure, the simulations are performed on a 0.5-mm grid.

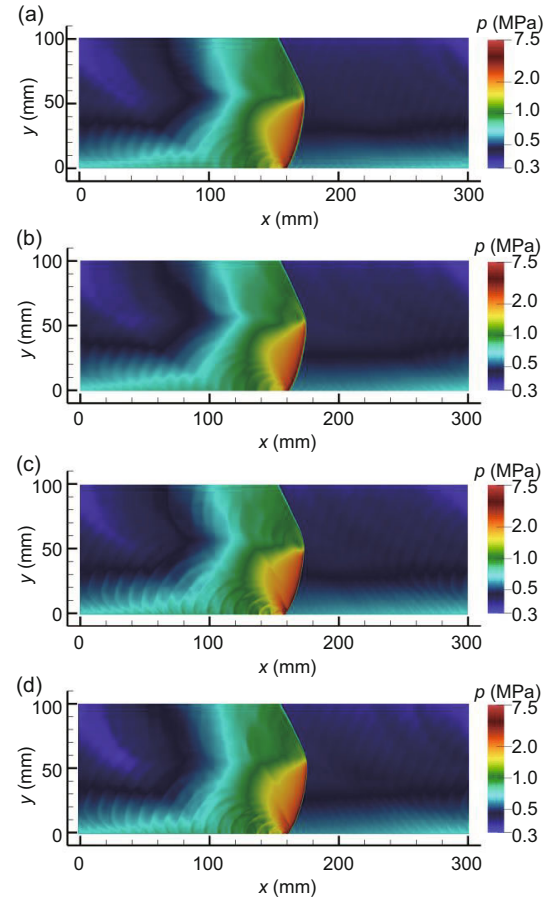


**Fig. 3** Comparison of the pressure contours computed on different systems: (a) 0.5-mm grid size,  $t = 1196 \mu\text{s}$ ; (b) 0.5-mm grid size,  $t = 2217 \mu\text{s}$ ; (c) 0.2-mm grid size,  $t = 1196 \mu\text{s}$ ; (d) 0.2-mm grid size,  $t = 2217 \mu\text{s}$

### 3.2 Stable operational mode of RDE

Recently, multiplicity phenomena have been widely studied in rotating detonation combustors. The one-wave operational mode of RDEs is known to be quite stable. As the filling height of the fuel increases or the mixture becomes more reactive, more waves will likely be generated in the engine (George et al., 2017). The boundaries demarcating the different operational modes are determined by the engine design parameters. To predict and control the operational modes of an RDE, we must investigate the factors inducing operational mode transition. To achieve this goal, the engine is initiated in different operational modes (different numbers of initial DWs). Various evolution processes are observed and analyzed for a constant molar ratio of the premixed hydrogen, oxygen, and nitrogen gases (2 : 1 : 7).

The final operational modes of the engine for

different numbers of initial DWs (defined as  $N_{\text{initial}}$ ) are shown in Table 2. Under the traditional single-ignition condition (case A), the single-wave operational mode is not maintained, because new DW fronts are spontaneously formed during the evolution process (Fig. 4a). The engine finally operates in the four-wave mode, with four DWs traveling in the same direction through the combustion chamber. When two initial DWs are initiated in the chamber (case B), both DWs propagate stably from the beginning to the end of the simulation (Fig. 4b). Only some waxing and waning instability (Anand et al., 2015) is observed. The number of DWs in the fully developed detonation flow matches that in the initial flow. The evolution process with three initial DWs (case C) resembles that of case B. Increasing the number of DWs decreases the height and velocity of the DWs. Bykovskii et al. (2005) and Yao and Wang (2016) reported the same trend in their experimental and numerical studies.

As indicated in the above results, the number of initial DWs affects the evolution process of the flow field and plays an important role in determining the final operational mode of the engine. Similar results

**Table 2 Simulated detonation velocities for different numbers of initial DWs**

Case	$N_{\text{initial}}$	Operational mode	$u_{\text{DW}}$ (m/s)
A	1	Four-wave	1403.0
B	2	Two-wave	1437.5
C	3	Three-wave	1421.5

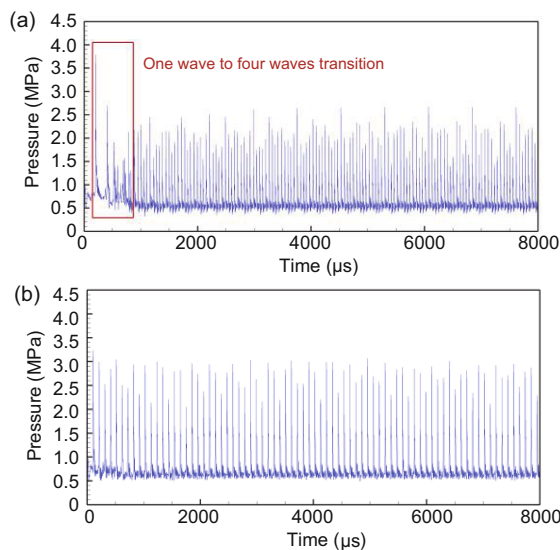


**Fig. 4 Pressure traces from 0 to 8000  $\mu\text{s}$  at the point  $x = 160 \text{ mm}$ ,  $y = 10 \text{ mm}$ : (a) case A; (b) case B**

were reported by Yao and Wang (2016). To understand the underlying mechanism of this phenomenon and to predict the transient changes in the flow field, we present the details of the evolution process in the following subsection.

### 3.3 Evolution process of the flow field

#### 3.3.1 Four-wave mode

A single initial DW cannot stably propagate and spontaneously initiate new DWs. According to the flow-field characteristics, the evolution process can be divided into three stages: the initial, unstable, and stable stages.

##### 1. Initial stage

Figs. 5a–5c show the pressure contours during the initial stage, which lasts from 0 to 476  $\mu\text{s}$ . Because the film is reasonably pre-filled, DW is rapidly established in the combustion chamber. The single DW dominates the flow field up to 476  $\mu\text{s}$ .

##### 2. Unstable stage

In the unstable stage (lasting from 512 to 780  $\mu\text{s}$ ), DWs are spontaneously formed and interacted with each other. Two intense compression waves are spontaneously formed at 512  $\mu\text{s}$ , and are clearly visible in Fig. 5d. Both compression waves subsequently develop into DWs (Figs. 5e and 5f). During the short formation period of the new DWs (512–532  $\mu\text{s}$ ), four important features of the flow field appear, from which we deduce a plausible underlying mechanism of the transition phenomenon. (1) Fuel injection and nonuniform fuel distribution cause pressure fluctuations in the  $x$  direction near the inlet. These weak waves (labeled by arrows in Fig. 5c) are visible throughout the evolution process. (2) Depending on the injector installation position, the fresh mixture is directly injected into the detonation products, funneling the distribution of the reactive mixture (Fig. 6a) (p.728). (3) Chemical reactions occur on the contact surface, defined as the area separating the detonation product from the fresh mixture (Fig. 6a). As evidenced in Fig. 6b, the chemical reaction rates on the contact surface are inconsistent, being high at the position indicated by the arrow. The chemical reaction intermediates (such as OH) tend to concentrate in the area between two fuel injection areas (Fig. 6c). (4) Newly formed DWs originate inside the reactive mixture, and two strong compression waves are closely combined with their

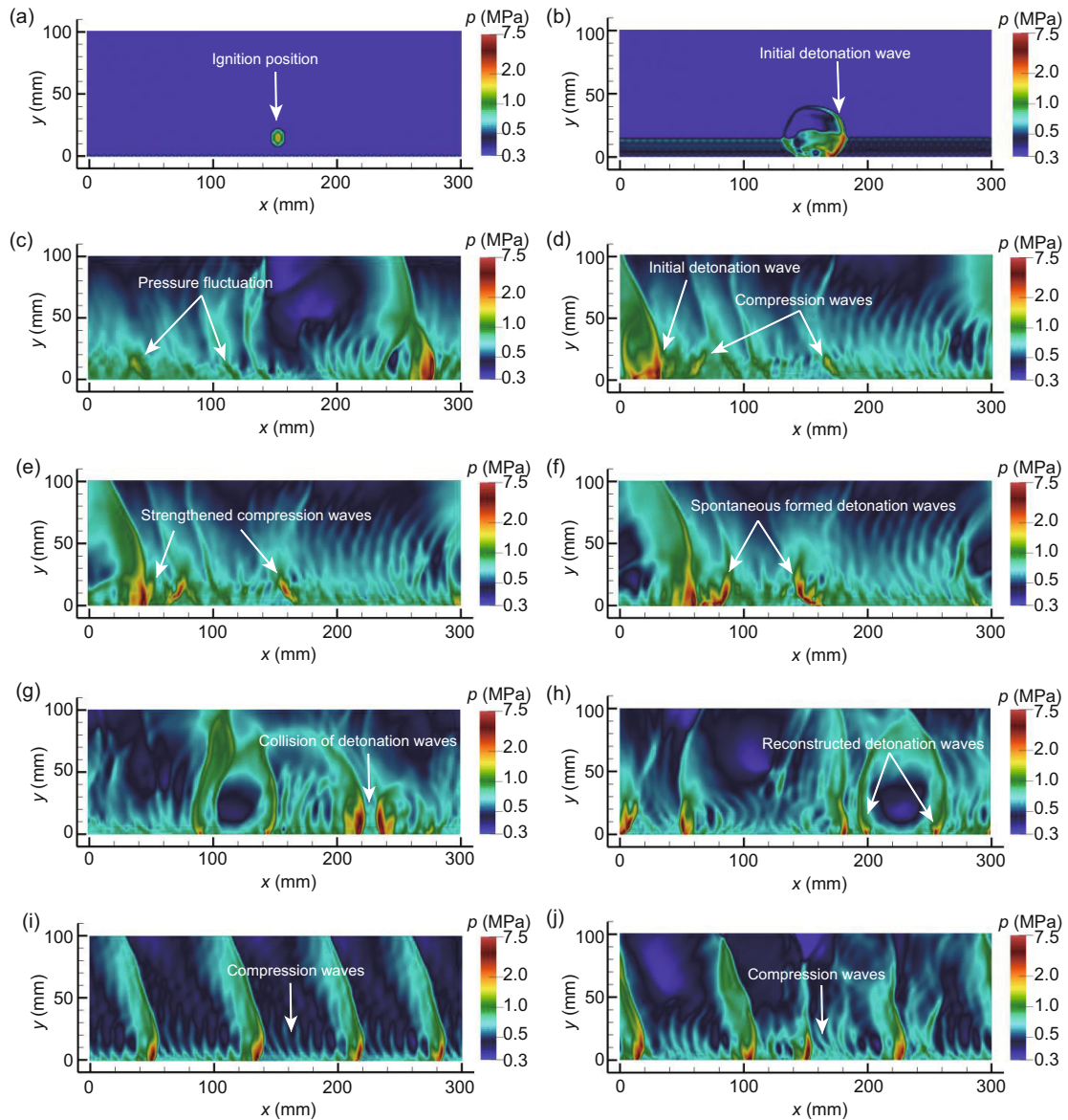


**Fig. 5** Pressure contours in case A: (a)  $t = 2 \mu\text{s}$ ; (b)  $t = 20 \mu\text{s}$ ; (c)  $t = 476 \mu\text{s}$ ; (d)  $t = 512 \mu\text{s}$ ; (e)  $t = 522 \mu\text{s}$ ; (f)  $t = 532 \mu\text{s}$ ; (g)  $t = 578 \mu\text{s}$ ; (h)  $t = 608 \mu\text{s}$ ; (i)  $t = 780 \mu\text{s}$ ; (j)  $t = 1916 \mu\text{s}$

corresponding chemical reactions. This coupling is confirmed by the coincidence of the peak pressure and peak OH mass fraction (Fig. 7). Features (1) to (3) indicate that the flow field accelerates the chemical reaction. More importantly, the above four features are consistent with the characteristics of deflagration-to-detonation transitions (DDTs) in flow fields, as summarized by Oran and Gamezo (2007). Therefore, we speculate that new DWs spontaneously form when DDTs occur via chemical reactions at the contact surface. A similar phenomenon was observed by Schwinn et al. (2018) in

their experimental study of an “unwrapped” RDE configuration. They referred to the phenomenon as “auto-ignition.”

Chemical reactions on the contact surface also change the fuel accumulation in front of the DWs. The height of the fuel layer ( $H_2$ ) initially increases after the fuel injection, and then decreases as the fuel is excessively consumed by the surface chemical reaction. Fig. 8 plots the height of  $H_2$  layer ( $h$ ) versus time at the section  $x = 74 \text{ mm}$  in Fig. 6a. The initial time point is set at  $t = 348 \mu\text{s}$  when the last DW leaves  $x = 74 \text{ mm}$  and fuel begins to

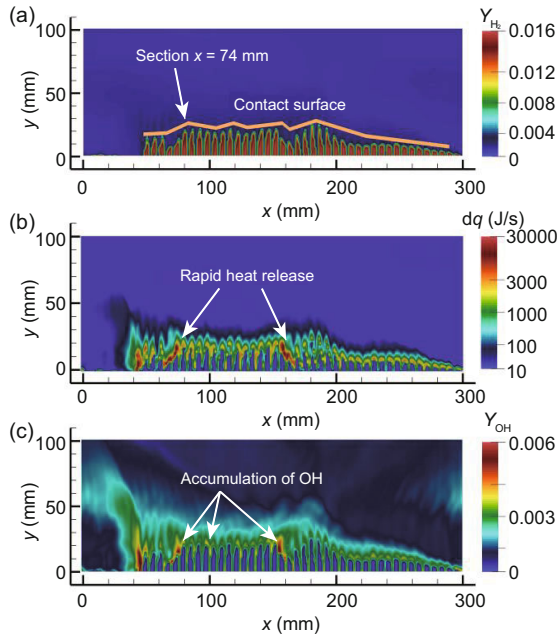


**Fig. 6** Instantaneous distributions of hydrogen mass fraction, heat release contours, and OH mass fraction in an RDE combustor at  $t = 522 \mu\text{s}$ : (a) hydrogen mass fraction contours; (b) heat release contours; (c) OH mass fraction contours

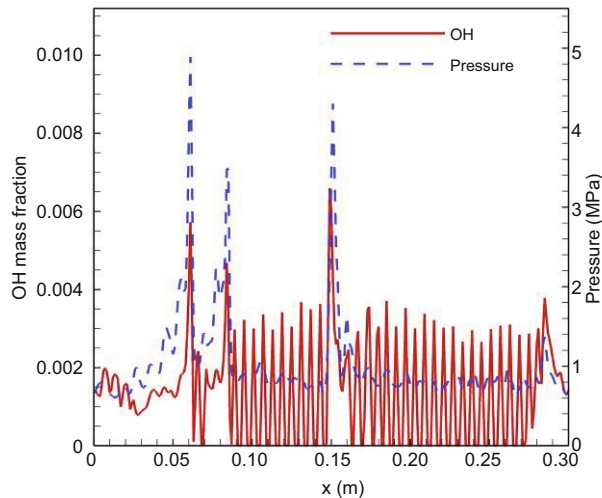


**Fig. 7** Pressure distribution and OH mass fraction distribution along the  $x$  direction at  $532 \mu\text{s}$

accumulate. At time  $t_W$ , the fuel height accumulates to  $h_{cr}$ . After time  $t_L$ , the fuel height drops below  $h_{cr}$ . The physical meaning of  $h_{cr}$  will be discussed in Section 3.4.1. Note that the evolutionary regularity depicted in Fig. 8 is not limited to  $x = 74 \text{ mm}$ , but is a typical behavior in the combustor.

The spontaneously formed DWs collide with other DWs and are quenched. At  $578 \mu\text{s}$ , several DWs appear in the combustor (Fig. 5g). During

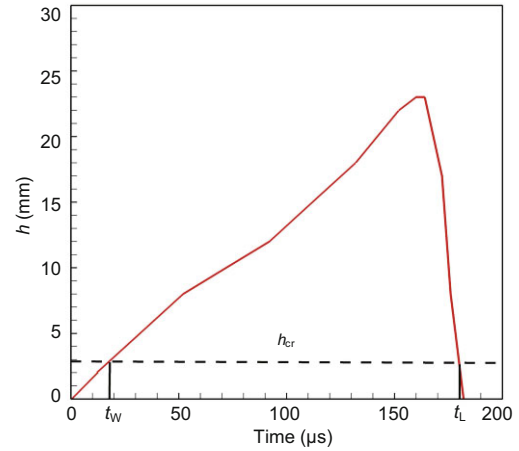


**Fig. 8** Height of fuel layer versus time at section  $x = 74 \text{ mm}$

this period, the flow is quite unstable and unpredictable. Due to their different intensities, some DWs are rapidly reconstructed under the transmission shock-wave interaction (Figs. 5g and 5h). These reconstructions extend the stabilization process and complicate the flow-field prediction.

### 3. Stable stage

After spontaneous formation of DWs and their subsequent collisions, quenching, and reconstructions, the flow field gradually settles into the stable stage. At  $780 \mu\text{s}$ , DWs propagate stably again with a consistent number of DWs propagating in the same direction (Fig. 5i). The four DWs propagate from left to right, almost identically to that in the experimental study of Frolov et al. (2015), where an operational mode with four DWs was established by one initial DW.

#### 3.3.2 Two- and three-wave modes

Fig. 9 shows the evolution of the flow field with two initial DWs ( $N_{\text{initial}} = 2$ ) formed after ignition. Both DWs propagate from left to right. Unlike case A, these initial DWs are stable and no DW is spontaneously formed in the combustion chamber. The unstable stage described in the previous subsection is absent in case B. The three-wave mode (case C) exhibits the same quasi-steady process (Fig. 10), with three initial DWs propagating stably from the beginning to the end of the simulation.

As shown above, the chemical reactions occurring on the contact surface can trigger the spontaneous formation of DWs, and then cause unstable mode transformations. We thus divide the evolution

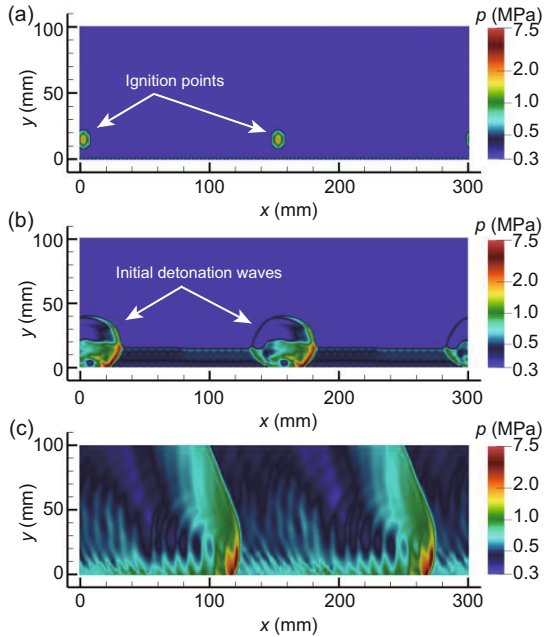


**Fig. 9** Pressure contours in case B (two initial DWs): (a) 2  $\mu\text{s}$ ; (b) 20  $\mu\text{s}$ ; (c) 1000  $\mu\text{s}$

process in an RDE into two categories, “quasi-steady evolution” and “unstable evolution.” In quasi-steady evolution, all initial DWs propagate stably and the chemical reactions on the contact surface cannot trigger new DWs. The fully developed detonation flow contains the same number of DWs as that in the initial condition. In contrast, unstable evolution is characterized by the formation of new DWs, collisions between DWs, and the DW quenching during the stabilization process. Accordingly, the number of DWs changes throughout the simulation.

### 3.4 Stability of rotating detonation waves

In our simulations, the rotating detonation flow is stable when the number of DWs exceeds a certain value. Anand et al. (2015) confirmed this general trend in their experimental study. However, the number of DWs needs to be quantitatively related to the stability of the flow field. In Section 3.3, we explained the underlying mechanism of the spontaneous formation of DW fronts. Through the above analysis, we can predict the stability of the rotating detonation flow field to some extent.

#### 3.4.1 Prediction of operational mode transitions

Previous studies have linked the stability of DWs to the fuel layer in front of DWs (Voitsekhovskii,

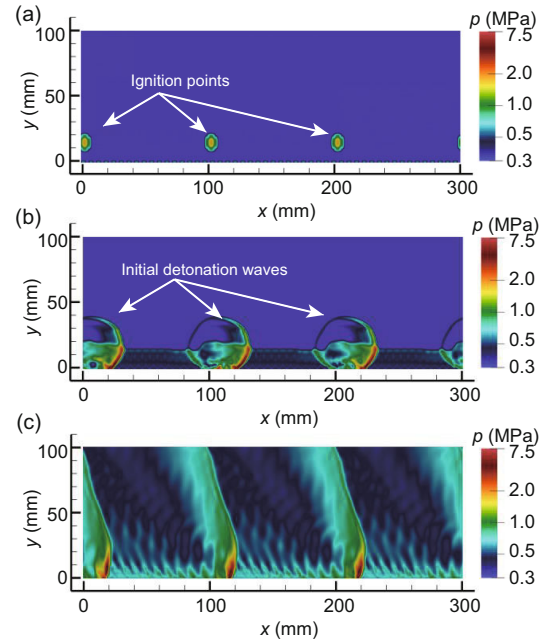


**Fig. 10** Pressure contours in case C (three initial DWs): (a) 2  $\mu\text{s}$ ; (b) 20  $\mu\text{s}$ ; (c) 1000  $\mu\text{s}$

1959; Daniau et al., 2005; Wolański, 2011; Anand et al., 2016). Above some critical height  $h_{cr}$  of the fuel layer  $h$  ahead of the DWs, the DWs can propagate stably and multi-detonation waves are encouraged (Daniau et al., 2005; Wolański, 2011; Anand et al., 2016). At fuel-layer heights below  $h_{cr}$ , the DWs will be quenched or extinguished (Daniau et al., 2005; Wolański, 2011). The value of  $h_{cr}$  is determined by the sensitivity of the mixture to detonation (Voitsekhovskii, 1959) and can be empirically calculated as

$$h_{cr} \approx (12 \pm 5)\lambda, \quad (15)$$

where  $\lambda$  is the detonation cell size.

As the chemical reaction of the contact surface accelerates (Section 3.3.1), the height of the fuel layer first increases and then decreases. The fuel height changes at two important time nodes,  $t_W$  and  $t_L$ . The time  $t_W$  defines the time during which the fuel height accumulates to  $h_{cr}$  after the fresh mixture is completely consumed somewhere near the inlet. More important is the time  $t_L$ , during which fuel is consumed to a height below  $h_{cr}$ . For instance, at section  $x = 74$  mm in the combustor of case A (Fig. 6a), the height of the fuel layer varies (Fig. 8). From  $t_W$  to  $t_L$ , the fuel layer is higher than the critical height. If the time  $t_T$  at which DW reaches section  $x = 74$  mm is located between  $t_W$  and  $t_L$ , the excessive acceleration of the chemical reaction on the contact surface

is avoided, and the DWs evolve in the quasi-steady state, as observed in case A for four DWs. Otherwise, the evolution is unstable, as observed in case A for a single DW. The premise condition of quasi-steady evolution of DWs is thus given by

$$t_W \leq t_T \leq t_L. \quad (16)$$

For simplicity, the DWs are supposed to be evenly spaced in the combustion chamber. The premise condition of quasi-steady evolution is then expressed as

$$t_W \leq \frac{L}{u_{DW}N_{DW}} \leq t_L, \quad (17)$$

where  $u_{DW}$  is the average DW velocity,  $L$  is the average perimeter of the annular combustion chamber, and  $N_{DW}$  is the number of DWs in the combustion chamber. The stable propagation of a DW depends on the relationships among  $L$ ,  $u_{DW}$ ,  $N_{DW}$ ,  $t_W$ , and  $t_L$ . To relate the number of DWs  $N_{DW}$  to the stability of the flow field, we introduce two dimensionless parameters  $N_W$  and  $N_L$  as

$$N_W = \frac{L}{u_{DW}t_W}, \quad (18)$$

$$N_L = \frac{L}{u_{DW}t_L}. \quad (19)$$

To ensure quasi-steady evolution, we deduce that the number of DWs must satisfy

$$N_L \leq N_{DW} \leq N_W. \quad (20)$$

If Eq. (20) is initially satisfied, the DWs can propagate stably and their number will be fixed. Otherwise, the number of DWs will change until Eq. (20) is satisfied. Eq. (20) explains the evolution processes described in Section 3.3. Beyond some critical number  $N_L$ , the DWs evolve in the quasi-steady state; that is, they propagate stably and dominate the flow field. When the DWs are fewer than  $N_L$ , their evolution is unstable, leading to a spontaneous formation of new DWs and an unstable flow field. Thus, by comparing the number of DWs with  $N_L$ , we can predict the subsequent evolution process. In the special but common situation  $N_L \leq 1$ , the contact-surface chemical reaction is too weak to destabilize even a one-wave mode. The proposed dimensionless parameter  $N_L$  indicates that a minimum number of DWs can maintain stable evolution in a given engine.

Moreover, at the maximum number of DWs that sustain stable evolution,  $N_W$  has the same physical meaning as  $W$  proposed by Wolański (2011). This observation is not further discussed in this study.

#### 3.4.2 Verification and application of $N_L$ in the engine

The value of  $N_L$  is influenced by the engine design parameters, such as injector resistance to back-flow, acoustic modes, total pressure and temperature of the injection, geometries of the combustion chamber, and operational conditions. The quantitative relationships between  $N_L$  and the design parameters must be determined in a future study. To verify Eq. (20) and demonstrate the applicability of  $N_L$ , we redesign the engine, reducing the width of its mixture inlets (Fig. 1) from 4 to 2 mm while maintaining fixed values of the other parameters. The  $N_L$  value of the newly designed engine is around 3.6. According to Eq. (20), the final stable operation stage of this engine should contain at least four DWs. Specifically, when the number of DWs in the combustor is less than 3.6, the subsequent process should be unstable evolution; conversely, when the number of DWs in the combustor exceeds 3.6, the subsequent process should be quasi-steady evolution.

Table 3 shows the simulation results for different numbers of initial DWs. Here,  $N_{\text{final}}$  is the number of DWs in the final stable stage. As predicted by Eq. (20), one, two, and three initial DWs ( $N_{DW} < N_L$ ) lead to an unstable evolution mode in which new DWs are spontaneously formed until their number reaches four or higher in the fully developed flow. Note that in case E, both the number of DWs and the propagation direction of the DWs differ from those in the initial condition. The evolution process in this case is shown in Fig. 11. After a long unstable stage (from 226 to 480  $\mu\text{s}$ ), a steady four-wave mode is established. A similar inversion of the propagation direction was reported in experimental studies (Bykovskii et al., 2006; Xie et al., 2018). When the number of initial DWs reaches four (exceeding  $N_L =$

**Table 3 Parameters and results of the simulations**

Case	$N_{\text{initial}}$	$N_L$	$N_{\text{final}}$	Evolution mode
D	1	3.6	4	Unstable
E	2	3.6	4	Unstable
F	3	3.6	6	Unstable
G	4	3.6	4	Quasi-steady

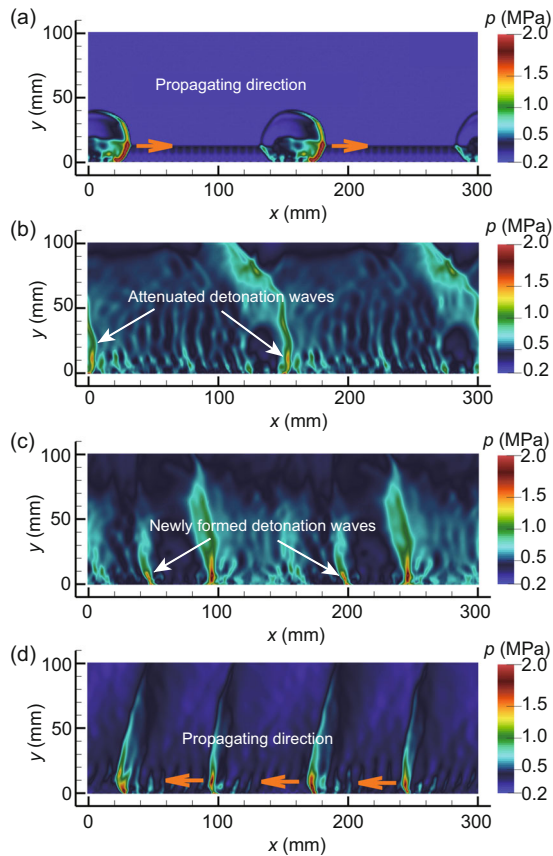


**Fig. 11** Pressure contours in case E (unstable evolution): (a)  $t = 20 \mu\text{s}$ ; (b)  $t = 226 \mu\text{s}$ ; (c)  $t = 306 \mu\text{s}$ ; (d)  $t = 698 \mu\text{s}$

3.6), the evolution enters the quasi-steady mode. In case G, the initial four DWs propagate stably and the flow field evolves as shown in Fig. 12.

From Eq. (20), it can be inferred that in engines with a high  $N_L$  number and few initial DWs, the stability of the rotating detonation flow field can be strengthened by increasing the number of DWs. This inference can explain the experimental findings of Anand et al. (2015), who reported a strengthened stability in a rotating detonation engine with an increase in the number of DWs. Eq. (20) also implies that the number of DWs can be increased by increasing the combustor perimeter. This inference was verified in a recent experimental study by Bykovskii et al. (2017), who evaluated the influences of the combustor diameter and length as scale factors.

The above discussion highlights the effectiveness of  $N_L$  in predicting the operational mode transitions induced by chemical reactions at the contact surface. By calculating the  $N_L$  value of the engine and selecting a reasonable number of ignition positions,

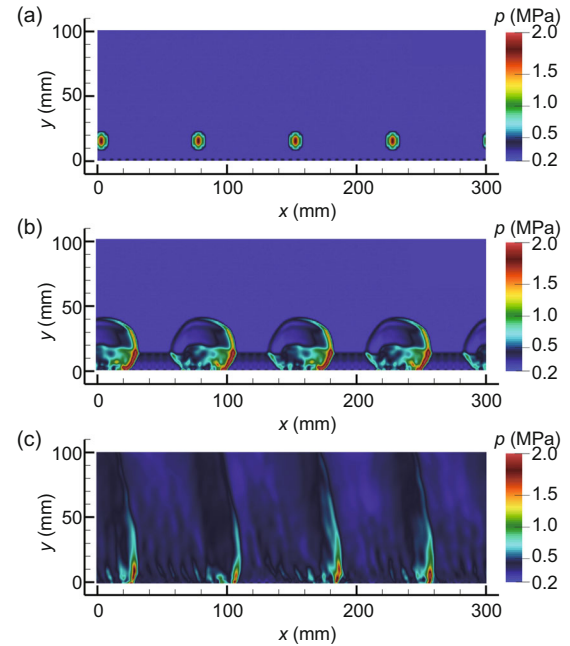


**Fig. 12** Pressure contours in case G (quasi-steady evolution): (a)  $t = 2 \mu\text{s}$ ; (b)  $t = 20 \mu\text{s}$ ; (c)  $t = 1996 \mu\text{s}$

the desired multiwave propagation mode can be obtained without transforming the operational modes in the detonation flow field. In addition, as the engine design parameters determine the value of  $N_L$ , they can be adjusted to increase  $N_L$ , and hence, the number of DWs in the combustion chamber.

## 4 Conclusions

This study relates the number of DWs in an RDE combustor to the stability of the rotating detonation flow field in a numerical simulation with a detailed chemical reaction model. The simulations reveal that the chemical reactions on the contact surface accelerate over time. The accelerated chemical reactions consume the fuel prepared for the coming DW, and can potentially trigger deflagration-to-detonation transitions that induce new DWs. When new DWs are formed, the flow field becomes highly unstable. In this study, RDE operates more stably when the number of DWs exceeds a certain value. This phenomenon has been observed but not explained in previous RDE experiments. To predict such unstable operational mode changes before they occur, we propose a parameter called  $N_L$ . If fewer than  $N_L$  DWs exist in the combustor, an unstable operational mode change is inevitable.

## Contributors

Pei-fen WENG, Xiao-quan YANG, Jue DING, and Zhi-di LEI designed the research. Zhi-di LEI and Zheng-wu CHEN processed the corresponding data. Zhi-di LEI drafted the manuscript. Xiao-quan YANG helped organize the manuscript. Jue DING revised and finalized the paper.

## Conflict of interest

Zhi-di LEI, Zheng-wu CHEN, Xiao-quan YANG, Jue DING, and Pei-fen WENG declare that they have no conflict of interest.

## References

- Anand V, George AS, Driscoll R, et al., 2015. Characterization of instabilities in a rotating detonation combustor. *International Journal of Hydrogen Energy*, 40(46):16649-16659. <https://doi.org/10.1016/j.ijhydene.2015.09.046>
- Anand V, George AS, Driscoll R, et al., 2016. Investigation of rotating detonation combustor operation with H<sub>2</sub>-air mixtures. *International Journal of Hydrogen Energy*, 41(2):1281-1292. <https://doi.org/10.1016/j.ijhydene.2015.11.041>
- Bader G, Deuffhard P, 1983. A semi-implicit mid-point rule for stiff systems of ordinary differential equations. *Numerische Mathematik*, 41(3):373-398. <https://doi.org/10.1007/BF01418331>
- Bykovskii FA, Vedernikov EF, 1996. Self-sustaining pulsating detonation of gas-mixture flow. *Combustion, Explosion and Shock Waves*, 32(4):442-448. <https://doi.org/10.1007/BF01998496>
- Bykovskii FA, Zhdan SA, Vedernikov EF, 2005. Continuous spin detonation in annular combustors. *Combustion, Explosion and Shock Waves*, 41(4):449-459. <https://doi.org/10.1007/s10573-005-0055-6>
- Bykovskii FA, Zhdan SA, Vedernikov EF, 2006. Continuous spin detonations. *Journal of Propulsion and Power*, 22(6):1204-1216. <https://doi.org/10.2514/1.17656>
- Bykovskii FA, Zhdan SA, Vedernikov EF, et al., 2017. Scaling factor in continuous spin detonation of syngas-air mixtures. *Combustion, Explosion, and Shock Waves*, 53(2):187-198. <https://doi.org/10.1134/S0010508217020095>
- Daniau E, Falempin F, Zhdan S, 2005. Pulsed and rotating detonation propulsion systems : first step toward operational engines. AIAA/CIRA 13th International Space Planes and Hypersonics Systems and Technologies Conference, Article 3233. <https://doi.org/10.2514/6.2005-3233>
- Deng L, Ma H, Xu C, et al., 2018. The feasibility of mode control in rotating detonation engine. *Applied Thermal Engineering*, 129:1538-1550. <https://doi.org/10.1016/j.applthermaleng.2017.10.146>
- Falempin F, Naour BL, 2009. R&T effort on pulsed and continuous detonation wave engines. 16th AIAA/DLR/DGLR International Space Planes and Hypersonic Systems and Technologies Conference, Article 7284. <https://doi.org/10.2514/6.2009-7284>
- Frolov SM, Aksenov VS, Ivanov VS, et al., 2015. Large-scale hydrogen-air continuous detonation combustor. *International Journal of Hydrogen Energy*, 40(3):1616-1623. <https://doi.org/10.1016/j.ijhydene.2014.11.112>
- Fujii J, Kumazawa Y, Matsuo A, et al., 2017. Numerical investigation on detonation velocity in rotating detonation engine chamber. *Proceedings of the Combustion Institute*, 36(2):2665-2672. <https://doi.org/10.1016/j.proci.2016.06.155>
- Gamezo VN, Desbordes D, Oran ES, 1999. Formation and evolution of two-dimensional cellular detonations. *Combustion and Flame*, 116(1-2):154-165. [https://doi.org/10.1016/S0010-2180\(98\)00031-5](https://doi.org/10.1016/S0010-2180(98)00031-5)
- George AS, Driscoll R, Anand V, et al., 2017. On the existence and multiplicity of rotating detonations. *Proceedings of the Combustion Institute*, 36(2):2691-2698. <https://doi.org/10.1016/j.proci.2016.06.132>
- Ginsberg T, Ciccarelli G, Boccio J, 1994. Initial hydrogen detonation data from the high-temperature combustion facility. Water Reactor Safety Information Meeting, Article BNL-NUREG-61445.
- Hippler H, Neunaber H, Troe J, 1995. Shock wave studies of the reactions HO+H<sub>2</sub>O<sub>2</sub>→H<sub>2</sub>O+HO<sub>2</sub> and HO+HO<sub>2</sub>→H<sub>2</sub>O+O<sub>2</sub> between 930 and 1680 K. *The Journal of Chemical Physics*, 103(9):3510-3516. <https://doi.org/10.1063/1.470235>
- Kurganov A, Noelle S, Petrova G, 2001. Semidiscrete central-upwind schemes for hyperbolic conservation laws and Hamilton-Jacobi equations. *SIAM Journal on Scientific Computing*, 23(3):707-740. <https://doi.org/10.1137/S1064827500373413>
- Li BX, Wu YW, Weng CS, et al., 2018. Influence of equivalence ratio on the propagation characteristics of rotating detonation wave. *Experimental Thermal and Fluid Science*, 93:366-378. <https://doi.org/10.1016/j.expthermflusci.2018.01.014>
- Lin W, Zhou J, Liu SJ, et al., 2015. Experimental study on propagation mode of H<sub>2</sub>/air continuously rotating detonation wave. *International Journal of Hydrogen Energy*, 40(4):1980-1993. <https://doi.org/10.1016/j.ijhydene.2014.11.119>
- Marinov NM, 1995. Transport Phenomena in Combustion. Taylor & Francis Group, USA.
- Naples A, Hoke J, Karnesky J, et al., 2013. Flowfield characterization of a rotating detonation engine. 51st AIAA Aerospace Sciences Meeting Including the New Horizons Forum and Aerospace Exposition, Article 278.
- Nordeen CA, Schwer D, Schauer F, et al., 2016. Role of inlet reactant mixedness on the thermodynamic performance of a rotating detonation engine. *Shock Waves*, 26(4):417-428. <https://doi.org/10.1007/s00193-015-0570-7>
- Oran ES, Gamezo VN, 2007. Origins of the deflagration-to-detonation transition in gas-phase combustion. *Combustion and Flame*, 148(1-2):4-47. <https://doi.org/10.1016/j.combustflame.2006.07.010>
- Oran ES, Weber Jr JW, Stefaniw EI, et al., 1998. A numerical study of a two-dimensional H<sub>2</sub>-O<sub>2</sub>-Ar detonation using a detailed chemical reaction model. *Combustion and Flame*, 113(1-2):147-163. [https://doi.org/10.1016/S0010-2180\(97\)00218-6](https://doi.org/10.1016/S0010-2180(97)00218-6)

- Peng L, Wang D, Wu XS, et al., 2015. Ignition experiment with automotive spark on rotating detonation engine. *International Journal of Hydrogen Energy*, 40(26):8465-8474.  
<https://doi.org/10.1016/j.ijhydene.2015.04.126>
- Schwer D, Kailasanath K, 2011. Numerical investigation of the physics of rotating-detonation-engines. *Proceedings of the Combustion Institute*, 33(2):2195-2202.  
<https://doi.org/10.1016/j.proci.2010.07.050>
- Schwinn K, Gejji R, Kan B, et al., 2018. Self-sustained, high-frequency detonation wave generation in a semi-bounded channel. *Combustion and Flame*, 193:384-396.  
<https://doi.org/10.1016/j.combustflame.2018.03.022>
- Sod GA, 1978. A survey of several finite difference methods for systems of nonlinear hyperbolic conservation laws. *Journal of Computational Physics*, 27(1):1-31.  
[https://doi.org/10.1016/0021-9991\(78\)90023-2](https://doi.org/10.1016/0021-9991(78)90023-2)
- Voitsekhovskii BV, 1959. Stationary spin detonation. *Soviet Journal of Applied Mechanics and Technical Physics*, 129:157-164.
- Wang C, Liu WD, Liu SJ, et al., 2015. Experimental investigation on detonation combustion patterns of hydrogen/vitiated air within annular combustor. *Experimental Thermal and Fluid Science*, 66:269-278.  
<https://doi.org/10.1016/j.expthermflusci.2015.02.024>
- Wolański P, 2011. Rotating detonation wave stability. 23rd International Colloquium on the Dynamics of Explosions and Reactive Systems, p.24-29.
- Wu D, Zhou R, Liu M, et al., 2014. Numerical investigation of the stability of rotating detonation engines. *Combustion Science and Technology*, 186(10-11):1699-1715.  
<https://doi.org/10.1080/00102202.2014.935641>
- Xie QF, Wen HC, Li WH, et al., 2018. Analysis of operating diagram for H<sub>2</sub>/air rotating detonation combustors under lean fuel condition. *Energy*, 151:408-419.  
<https://doi.org/10.1016/j.energy.2018.03.062>
- Yao SB, Wang JP, 2016. Multiple ignitions and the stability of rotating detonation waves. *Applied Thermal Engineering*, 108:927-936.  
<https://doi.org/10.1016/j.applthermaleng.2016.07.166>
- Yao SB, Liu M, Wang JP, 2015. Numerical investigation of spontaneous formation of multiple detonation wave fronts in rotating detonation engine. *Combustion Science and Technology*, 187(12):1867-1878.  
<https://doi.org/10.1080/00102202.2015.1067202>
- Yao SB, Han X, Liu Y, et al., 2017. Numerical study of rotating detonation engine with an array of injection holes. *Shock Waves*, 27(3):467-476.  
<https://doi.org/10.1007/s00193-016-0692-6>
- Zhang TT, Wang ZG, Huang W, et al., 2019. The overall layout of rocket-based combined-cycle engines: a review. *Journal of Zhejiang University-SCIENCE A (Applied Physics & Engineering)*, 20(3):163-183.  
<https://doi.org/10.1631/jzus.A1800684>

## 中文概要

**题目:** 旋转爆轰波传播模式自发改变过程研究

**目的:** 提出一种预测爆轰波传播模式自发改变的方法。

**创新点:** 1. 揭示了流场内新爆轰波产生的机制; 2. 基于接触面化学反应特征时间提出了无量纲参数 $N_L$ , 可作为分析旋转爆轰流场稳定性的判据。

**方法:** 以数值模拟为手段, 应用基元反应建立化学非平衡流动的数学物理模型, 开展旋转爆轰波传播稳定性研究。

**结论:** 1. 分界面化学反应是引起爆轰波传播模式自发转变的原因之一; 2. 提出的无量纲参数 $N_L$ 可以将模式转变与爆轰波数联系起来。

**关键词:** 旋转爆轰发动机; 基元反应; 多波传播模式; 爆轰稳定性